Published online 11 July 2017 *Nucleic Acids Research, 2017, Vol. 45, No. 15* ***8901–8915***
doi: 10.1093/nar/gkx593

Unencumbered Pol β lyase activity in nucleosome core particles

Yesenia Rodriguez[1], Michael J. Howard[1], Matthew J. Cuneo[2], Rajendra Prasad[1] and Samuel H. Wilson[1,*]

[1]From the Laboratory of Genome Integrity and Structural Biology, NIEHS-NIH, Research Triangle Park, NC 27709, USA and [2]Oak Ridge National Laboratory, Oak Ridge, TN 37831, USA

Received March 28, 2017; Revised June 23, 2017; Editorial Decision June 27, 2017; Accepted June 30, 2017

ABSTRACT

Packaging of DNA into the nucleosome core particle (NCP) is considered to exert constraints to all DNA-templated processes, including base excision repair where Pol β catalyzes two key enzymatic steps: 5′-dRP lyase gap trimming and template-directed DNA synthesis. Despite its biological significance, knowledge of Pol β activities on NCPs is still limited. Here, we show that removal of the 5′-dRP block by Pol β is unaffected by NCP constraints at all sites tested and is even enhanced near the DNA ends. In contrast, strong inhibition of DNA synthesis is observed. These results indicate 5′-dRP gap trimming proceeds unperturbed within the NCP; whereas, gap filling is strongly limited. In the absence of additional factors, base excision repair in NCPs will stall at the gap-filling step.

INTRODUCTION

DNA is surprisingly dynamic due to its susceptibility to a myriad of endogenous spontaneous and enzymatic reactions (1). Incorporation of permanent mutations may result in the activation of proto-oncogenes and/or inactivation of tumor suppressor genes, ultimately leading to cancer and other inborn diseases (2). To maintain genomic integrity, a number of specialized DNA repair pathways assist in the recognition and removal of DNA damage.

At the forefront, base excision repair (BER) plays an indispensable role in the maintenance of genomic stability as it repairs the vast majority of endogenous DNA lesions including damaged or aberrant DNA bases, apurinic/apyrimidinic (AP) sites, and single-strand breaks (2). It has been estimated that as many as 10 000 AP sites/cell/day can arise as a result of spontaneous hydrolytic reactions in human cells (3). Additionally, AP sites arise from enzymatic reactions initiated by several DNA glycosylases that remove chemically modified bases due to oxidation (e.g. reactive oxygen species), alkylation (e.g. S-adenosylmethionine), and incorporation of unnatural bases into DNA (1). The abundance of AP sites in the genome indicates that the BER pathway is highly active.

Biochemical characterization and structural crystallographic studies of BER enzymes have helped delineate the sequential steps and conformational changes necessary for catalysis during BER. The initial step of BER usually involves recognition and cleavage of the N-C1′ glycosydic bond between the deoxyribose sugar and the base by damage-specific DNA glycosylases (4). AP endonuclease 1 (APE1) cleaves the DNA backbone 5′ to the AP site, generating a single-nucleotide gap with 3′-OH and 5′-deoxyribose phosphate (dRP) at the margins of the gap (3). Under conditions where the 5′-dRP group is not chemically modified, repair proceeds via short-patch BER, and DNA Polymerase (Pol) β catalyzes removal of the 5′-dRP group and performs template-directed gap-filling. However, if the 5′-dRP is chemically modified, it may become refractory to Pol β's dRP lyase activity, promoting long-patch BER where 2–13 nucleotides are filled into a gap by Pol β or other DNA polymerases (5); the displaced DNA flap is cleaved by FEN1 with the assistance of other accessory factors. In the last step of BER, DNA Ligase I or Ligase III-XRCC1 complex seals the nick.

Pol β plays an indispensable role during single-nucleotide or short-patch BER by contributing 5′-dRP lyase activity. In fact, Pol β enzymatic activities are so crucial to an organism's survival that deletion of the gene encoding Pol β in mice leads to embryonic lethality (6). Pol β 5′-dRP lyase activity resides in the N-terminal 8-kDa domain (87 residues) (7), and the DNA gap-filling activity is located in the C-terminal 31-kDa domain (8,9). Characterization of these two domains revealed that the 31-kDa domain preferentially binds dsDNA, whereas the 8-kDa domain's DNA binding affinity is primarily for ssDNA (10,11). Although both domains can function independently of each other, the catalytic efficiencies of the isolated domains are reduced compared to the intact enzyme, suggesting that contacts between the domains are nonetheless important (10,12). However, studies performed with Pol β deficient mouse embry-

*To whom correspondence should be addressed. Tel: +1 919 541 3267; Fax: +1 919 541 3592; Email: wilson5@niehs.nih.gov

onic fibroblasts (MEFs) demonstrated that only the lyase activity of Pol β is necessary to reverse the methylating-agent induced hypersensitivity in these cells (13). This highlights the essential role of the dRP lyase activity *in vivo*. In humans, germline and somatic single nucleotide polymorphisms and variants have been found in many BER proteins, and some of these result in aberrant function. Importantly, Pol β variants, as well as its overexpression, have been linked to human cancers (14), underscoring the importance of understanding the molecular mechanisms that regulate Pol β activities.

The enzymatic activities of Pol β have been characterized *in vitro* with purified recombinant enzyme and DNA substrates; however, in living cells all DNA-templated processes are regulated by the chromatin landscape, where the nucleosome core particle (NCP) constitutes the primary level of this regulation. In the NCP, ∼147 bp of DNA wrap around an octameric complex composed of two copies of each of the core histones: H2A, H2B, H3, and H4 (15). Nucleosome cores are located in proximity to one another along chromosomes, separated by short variable lengths of 'linker' DNA ranging between 40 and 50 bp in humans (16). These 'beads on a string' structures are folded several thousand-fold to achieve a level of organization and compaction that allows for strategic control of all DNA-templated processes. This tight organization, however, poses an accessibility barrier where regions bound by histones are less accessible than the linker DNA. Considering that ∼83% of genomic DNA is occupied by histones (17) forming ∼30 million nucleosomes in each diploid human cell (18), the study of DNA-templated processes in the context of the NCP becomes biologically significant and a good model system. DNA lesions within NCPs are not completely refractory to repair, suggesting the NCP is intrinsically dynamic in the absence of external chromatin-modifying factors; however, the removal of many types of lesions can be inefficient (19–25).

As shown by *in vitro* studies, the structural determinants of the NCP that regulate BER repair are complex. This is because the NCP exhibits a spectrum of intrinsic interconnected dynamic mechanisms that can regulate DNA accessibility and enzyme activity in a site- and enzyme-specific manner (19,23,26,27). Consequently, not every enzyme or enzymatic reaction would encounter the same structural constraints at a specific site. Additionally, local structural features such as minor groove width may also play a role on lesion recognition and removal (25), and this is likely to depend upon an enzyme's active site interactions with the substrate. However, the extent to which the two major intrinsic parameters of the NCP (rotational and translational positioning) influence DNA repair have been generally correlated with the mode of binding to the NCP or extent of the local sculpting of the substrate necessary for catalysis (23,28).

As previously shown, rotational orientation near the dyad does not have the same effect on UDG and Pol β DNA synthesis activity (28). In fact, removal of outwardly oriented uracil can occur at a rate similar to that in free DNA (20,25). Similarly, the activity of APE1 is strongly regulated by the rotational orientation of the AP site, with faster repair for outwardly-oriented AP sites (21). Consequently, these results suggested that outwardly-oriented DNA gaps can be efficiently generated even in NCPs. Because UDG and APE1 primarily interact with the damaged DNA strand and the rotational orientation of the lesion in NCPs significantly influences lesion removal (20,22,25,28), we questioned whether the enzymatic activities of Pol β could be regulated by the NCP in a manner that is directly dependent on the extent of interactions mediated by each of the Pol β domains. Other studies had performed qualitative assessments of whether Pol β gap-filling occurs in the context of NCPs (19,29,30) and addressed structural factors influencing this activity (28). Quantitative kinetic measurements of the Pol β activities as a function of the NCP structural location are lacking. Recently, Howard *et al.* showed the NCP strongly inhibits Pol β gap-filling (∼500-fold) measured under single-turnover kinetic conditions. In this case, the nucleosomal substrate contained two single-nucleotide gaps located 17 bp apart (31). Another recent study containing translationally and rotationally positioned two-nucleotide gaps showed complete inhibition of Pol β, and this was modestly alleviated by the chromatin architectural factor HMGB1 (32). Importantly, the Pol β dRP lyase activity has not been characterized in the context of the NCP or whether the same structural rules for DNA gap-filling activity apply to the 5′-dRP removal.

The proposed mechanism for Pol β catalyzed dRP removal requires the formation of a Schiff base intermediate involving lysine72 as the main nucleophile, followed by the β-elimination reaction (33). There are many lysine residues present in histones, and whether or not they can catalyze a dRP lyase reaction may not only be dependent on proximity to the lesion but also on whether they are geometrically positioned or in a flexible region that would sterically allow the reaction (34). Crystallographic studies have proposed the need for significant structural rearrangements in order to position Pol β Lys72 and the 5′-dRP group in proximity so the dRP lyase reaction can occur (33). Similarly, significant structural rearrangements occur in gapped DNA upon Pol β binding, where the templating DNA strand is bent 90° upon pre-catalytic complex formation (35).

Considering all the structural requirements for Pol β's catalyzed enzymatic reactions, we sought to determine how the intrinsic structural features of the NCP regulate these activities. We quantified Pol β's NCP binding affinity and 5′-dRP lyase and DNA gap-filling activities in NCPs. In our binding assays, the results suggested that Pol β binds DNA non-specifically, and the histone octamer constitutes a significant steric barrier for stable binding. The dRP lyase assays demonstrated that full-length Pol β and the 8-kDa domain of Pol β are able to carry out 5′-dRP removal in NCPs. On the other hand, gap-filling by Pol β exhibits a very strong inhibition, in a manner that largely correlates with translational positioning of the lesion.

MATERIALS AND METHODS

Materials

Oligodeoxyribonucleotides (oligos) were from Integrated DNA Technologies (IDT) and all were individually PAGE purified. Each oligonucleotide was resuspended in DNase-, RNase-, protease-free water and the concentration was determined from the UV absorbance at 260 nm. Human

WT and mutant (K35A,K68A,K72A) Pol β were expressed in *Escherichia coli* (*E. coli*) and purified as previously described (33,36). Total enzyme concentrations were determined by the Bradford assay and are indicated within the plots or figure legends. *E. coli* uracil DNA glycosylase (UDG) was from New England Biolabs. All radiolabels (γ-^{32}P-ATP and 3′-α-^{32}P-dATP [cordicypin]) were from Perkin Elmer.

Preparation of DNA substrates containing single-nucleotide gaps

To generate each of the substrates containing the 147 bp Widom 601 DNA positioning sequence, the damaged strand contained phosphorylated deoxyuridine at the 5′ end of a DNA nick so that a 5′-deoxyribose phosphate (dRP) lyase substrate could be generated upon treatment with *Escherichia coli* UDG (Supplementary Table S1). The DNA nick with a 5′-dU was introduced at specific locations to allow for rotational positioning of the lesion when reconstituted into the NCP with the histone octamer. Oligomers were either 5′-end-labeled with γ-^{32}P-ATP (Perkin Elmer) using T4 polynucleotide kinase (Invitrogen) following the manufacturer's specifications or cordycepin and terminal deoxynucleotidyl transferase (Thermo Fisher). Figure legends describe which strand was labeled in each of the assays, where applicable.

After labeling the strand of interest, the dsDNA was generated by annealing two oligos to a complementary strand, in a 1:1:1 molar ratio, by heating to 95°C for 10 min and slow cooling in annealing buffer containing 10 mM Tris–HCl, pH 8, and 50 mM NaCl. Excess unincorporated radiolabel (γ-^{32}P-ATP or cordycepin) was removed using Biospin P-30 or P-6 chromatography columns (Biorad). As for previously reported nomenclature of the substrates (28), each substrate was named to indicate the type of lesion it contained: (i) 5′-deoxyribose phosphate (dRP), single-nucleotide gap (g), tetrahydrofuran (THF); (ii) the translational positioning of the damage on the DNA strand corresponding to the I chain of pdb file 3LZ0 (37), where the number in parenthesis indicates the number of nucleotides away from the dyad towards the 5′end (+) or 3′end (–) and (iii) the rotational orientation of the DNA backbone relative to the histone octamer surface (in, indicated by 'I' or out by 'O'). Rotational orientation for these substrates has been previously confirmed by hydroxyl radical footprinting for all substrates with a definitive rotational orientation (37). The substrate positioned 60 nucleotides from the dyad of the I chain is not stably rotationally positioned, given that the last 13 bp of DNA ends are more loosely associated with the histone octamer (38).

Nucleosome core particle reconstitution and characterization

Nucleosome core particles (NCPs) were reconstituted by salt gradient dialysis using the recombinant histone octamer from *Xenopus laevis* containing equimolar amounts of each of the core histones: H2A, H2B, H3, and H4. First, each histone was individually expressed in *E. coli* (BL21) as previously described (38) with the modifications described (39). After isolation, the histones were subjected to dialysis in 5 mM 2-mercaptoethanol and 0.2 mM PMSF. They were then lyophilized until dry, and the histone octamer was prepared as described by Luger *et al.* (40). Briefly, the concentration of the unfolded histone proteins was determined at A_{280}, and an equimolar ratio of all four histones was mixed and dialyzed four times in refolding buffer (2 M NaCl, 20 mM Tris–HCl, pH 7.5, 1 mM Na-EDTA, 5 mM 2-mercaptoethanol) at 4°C over the course of 48–72 h. The histone octamer was then concentrated and loaded onto a Superdex-S200 column (See Supplementary Figure S1A). Elution fractions were analyzed using a 16.5% Tris-Tricine Criterion protein gel (Biorad), and fractions containing equimolar concentrations of the histones were pooled (Supplementary Figure S1B), concentrated and stored in 50% glycerol at –20°C. The histone octamer was then used to reconstitute ^{32}P-radiolabeled DNA in a 1.2:1 (octamer:DNA) molar ratio via salt gradient dialysis, as previously described, with the exception that for the fluorescence anisotropy studies, the reconstitution buffers contained KCl (at the same respective concentrations as previously described (28) in the buffers with NaCl, i.e. 1 M, 600 mM and 50 mM); these solutions were devoid of NP-40 and supplemented to a final concentration of 1.6 mM CHAPS. NCP reconstitution efficiency was determined by electrophoretic mobility shift assay (EMSA) in a non-denaturing 6% polyacrylamide gel (Supplementary Figure S1C). Reconstitutions containing less than or equal to 5% free DNA and/or aggregates were used in all assays. To further characterize the substrates and to rule out contaminating free DNA in the NCP preparations, restriction enzyme accessibility assays were employed as previously described (See Supplementary Figure S1D). Briefly, restriction enzyme HhaI (New England Biolabs), which cleaves at a site corresponding to translational position 0, or the dyad of the I chain in the 601 NCP crystal structure, was used to determine accessibility of these sites. Undamaged DNA and NCPs were incubated with 10 units of HhaI in 1X Cutsmart New England Biolabs buffer (50 mM potassium acetate, 20 mM tris-acetate, 10 mM magnesium acetate, 100 μg/ml BSA) at 37°C for 2 h followed by standard phenol/chloroform extraction. Cleavage products were separated on a 12% non-denaturing polyacrylamide gel. The gels were then stained with SYBR green I for 5 min and rinsed five times with dH_2O. Using a Typhoon FLA9500 scanner, the gels were visualized and the image was analyzed by ImageQuant (IQ)TL v.8.1.

Pol β DNA and NCP binding assays: Gel mobility shift assay

Binding incubations were performed on ice for 10 min in a total volume of 10 μl per binding mixture. Each binding mixture contained a final concentration of 50 nM substrate (DNA or NCP), 50 mM Hepes, pH 7.5, 37 mM KCl, 5 mM $MgCl_2$, 0.5 mM EDTA, 100 μg/ml BSA and varying amounts of Pol β (0–6 μM final concentration). The binding mixtures were immediately subjected to non-denaturing 6% polyacrylamide gel (acrylamide:bis-acrylamide, 37.5:1) electrophoresis. To help maintain integrity of bound complexes during electrophoresis, the gel was run at 4°C. The gel was then stained with SYBR green I. Visualization and analyses were performed as described above. Because some of the bound signal was, in some cases, a smear rather than

a distinct band, the toolbox setting in IQTL v.8.1 was used to more accurately determine the signal in the smear after background subtraction from a box of the same size. The fraction bound relative to the total signal was then determined and plotted using Kaleidagraph v.4.1. The data were fitted to a modified Hill binding equation, where the fraction of substrate (DNA or NCP) bound is related to the K_d as described (41):

$$f = \left(\frac{f_{max} * [E]^n}{[E]^n + k_d} \right) + f_{min} \quad (1)$$

where f_{max} and f_{min} are normalization factors that represent the fraction of substrate bound at the highest and lowest asymptotes of the titration, [E] is the total enzyme concentration and n is the Hill coefficient. The Hill coefficient measures cooperativity of binding. Values larger than $n = 1$ may indicate positive cooperativity of multiple proteins or binding events that have not reached equilibrium. From the fitted data, independent of DNA damage and structural location within NCPs, values of $n = 2$ and $n = 3$ were derived from the fits for DNA and NCP, respectively. The estimated *K*d value for NCP-THF-O (–35) was verified by fluorescence anisotropy.

Pol β and NCP binding fluorescence anisotropy assay

Fluorescence anisotropy measurements were used to determine binding affinity of NCPs containing 5′-P-THF (–35) at the 5′ end of a nick, mimicking a single nucleotide gap with a stable 5′-dRP group. Exposed cysteine residues of Pol β were mutated to serine in order to site-specifically introduce the 5-iodoacetamidofluorescein fluorescent reporter group at residue 303 (V303C). Fluorescence anisotropy measurements were carried out on a Horiba FluoroLog Fluorimeter at 20°C in a buffer consisting of 50 mM Hepes, pH 7.5, 20 mM KCl, 2 mM DTT, 5 mM $MgCl_2$ and1.6 mM CHAPS with a final Pol β V303C concentration of 5 nM. The final concentrations of NCPs are given in the figure. The excitation and emission wavelengths were 485 and 520 nm, respectively, each with a 12-nm slit width. Fluorescence anisotropy change was fitted to one-site binding model with Origin 8.

Pol β enzymatic activity assays: dRP lyase assay

Assays were performed by two different approaches for product measurement: (i) traditional ^{32}P-3′-end labeling and (ii) direct labeling of the 5′-dRP group with ^{32}P. In both cases, the reaction conditions were identical, but separation of substrate and product differed significantly. ^{32}P-3′-end label reactions were resolved in a 6% polyacrylamide (19:1, acrylamide: bisacrylamide) 7 M urea denaturing gel at a constant 65 W in 1× TBE running buffer. 5′-^{32}P-dRP lyase assays allowed for efficient separation in a 20% 7 M urea denaturing gel.

In both types of assay, to generate the dRP lyase substrate, 400 nM substrate (DNA or NCP) was incubated at 37°C in reaction buffer containing a final concentration of 50 mM Hepes, pH 7.5, 20 mM KCl, 2 mM DTT, 5 mM EDTA, 40 μg/ml BSA and 1.7% glycerol. Addition of 493 U of *E.* coli UDG initiated the reaction. After 5.5 min incubation, three aliquots were taken: (i) heat control (indicated by 'H' in Figure 3), which was incubated at 75°C for 2 min to assess uracil removal and determine the actual amount of dRP lyase substrate, (ii) 0 time-point quenched immediately with 0.5 M $NaBH_4$ to a final concentration of 270 mM to determine spontaneous dRP loss during the UDG reaction at the initiation of the dRP lyase reaction and (iii) the remaining volume was mixed 1:1 (v/v) at 30°C (with a tube containing 50 nM full-length recombinant human Pol β, or 150 nM recombinant 8-kDa domain rat Pol β, or no Pol β, all in the same reaction buffer as for the UDG treatment, which were previously incubated for 1 min at 30°C before initiation of the reaction. Thus, the final total concentration for dRP lyase substrate in the reaction was 200 nM (DNA or NCP), and this value was normalized to the actual fraction determined by the heat control in 5′-dRP label assays or directly in the 3′-end label assay where the heat control was omitted. This value was used to determine the dRP product formation shown on the ordinate of the dRP lyase product formation plots. All reactions were quenched with 0.5 M $NaBH_4$ to a final concentration of 270 mM and placed on ice for 30 min. To remove proteins and isolate DNA from the histone octamer, samples were treated with phenol/chloroform (PCl) in a 1:2 (v/v) ratio of sample: PCI. The aqueous layer was then mixed 1:1 with 2× deionized formamide sample buffer (95% formamide, 0.025% (w/v) bromophenol blue, 0.025% (w/v) Xylene cyanol and 5 mM EDTA, pH 8). Samples were incubated for 2 min at 95°C and separated by electrophoresis as described above. In the case of DNA sequencing gels, they were transferred onto Whatman paper, dried, and exposed on a phosphor screen. DNA gels where the 5′-dRP was labeled were exposed without drying. Because the 5′-dRP group is heat labile, mock treated samples incubated with just the reaction buffer (-Pol β) were important controls to subtract the amount of product formed spontaneously over the course of the reaction, as later time points in the time-course, in some cases, exhibited a small increase in spontaneous dRP loss compared to the loss at 0 min time point. Data were plotted as described previously; the initial rate (v_0) was determined from the linear part of the time-course. The enzyme activities presented in the tables are the initial rate divided by the total enzyme concentration ($v_0/[E_{total}]$). Kinetic parameters are shown in Tables 2 and 3.

Pol β enzymatic activity assays: DNA synthesis assay

The strand upstream of the 5′-dU was radiolabeled at its 5′ end with [γ-^{32}P]-ATP using T4 polynucleotide kinase (Invitrogen). To generate the single-nucleotide gap, the nicked dsDNA was incubated with 63 U of *E. coli* UDG at 37°C for 2 hr in the buffer conditions described above for uracil removal. To remove UDG and quench the reaction, the sample was treated with PCI. The gapped DNA was then resuspended in dH_2O using an Illustra micro-spin G-25 column (GE). DNA concentration was determined by UV absorbance at 260 nm, and part of the sample was reconstituted with the histone octamer. For multiple turnover experiments, the reaction was performed manually by preparing two tubes with enzyme and substrate (which contained the

appropriate dNTP based on the templating base at a final 50 μM concentration) in BER reaction buffer (50 mM Hepes, pH 7.5, 100 mM KCl, 2 mM DTT, 100 μg/mL BSA and 5 mM $MgCl_2$ final concentrations). After 5 min incubation at 37°C, the reaction was initiated by mixing the substrate (500 nM final concentration) and Pol β. The final enzyme concentration is given in the figure legends of the plots, but in all cases was in limiting molar amounts relative to the substrate by at least 10-fold. Aliquots were taken, and the reaction was quenched with 100 mM EDTA to a final concentration of 89 mM. PCI extraction was then performed as described above, and extension products were separated. Data were plotted as described above and fitted to a single exponential equation:

$$Y = C + Y_{\max}(1 - e^{-k_{obs}t}) \quad (2)$$

as previously described (20). The initial rate of the reaction (v_0) was determined by taking the derivative of Equation (2) (dY/dt) as t approaches 0. The rate constant, ($v_0/[E_{\text{total}}]$), was then calculated as follows:

$$v_0/[E_{\text{total}}] = \frac{Y_{\max} * k_{\text{obs}}}{E_{\text{total}}} \quad (3)$$

Single turnover reactions were performed in a similar manner with the same buffer conditions, except that for all DNA samples, the reactions were performed using rapid quench flow with a KinTeK RQF3 apparatus. The final DNA substrate concentration in these reactions was 10 nM, and the Pol β concentration was 1 μM. The final concentration of all NCP reactions (performed manually) was 100 nM. Reaction mixtures were incubated at 37°C for the specified times. Processing of samples, separation, and data analyses were performed as described above, except that the observed single turnover rate constant (k_{obs}) was directly derived from the fits to Equation (2). Catalytic rate constants for DNA synthesis are summarized in Table 4.

RESULTS

Design of damaged nucleosome core particles and characterization

A total of four DNA substrates containing a single-nucleotide gap were compared in this study (Figure 1 and Supplementary Table S1). The structural location of the designed DNA lesions encompasses the two main structural constraints imposed by the NCP: rotational and translational positioning (Figure 1); these are included in the nomenclature of the substrates as described in Materials and Methods. Recognition and removal of BER lesions are largely dependent on the lesion's rotational and translational positioning within the NCP in reconstituted *in vitro* BER assays (23,26).

To accurately determine the effects of translational positioning on the Pol β dRP lyase reaction, we used the 147-bp 601 DNA strong positioning sequence and the recombinant histone octamer from *X. laevis* (Supplementary Figure S1A&B), both of which are known to generate stable well-positioned NCPs. As shown in Supplementary Figure S1C, all substrates were well positioned, independent of the location of the lesion in agreement with previous studies (28,42). Additionally, restriction enzyme accessibility assays of undamaged NCP resulted in the expected occlusion of the HhaI restriction site (Supplementary Figure S1D), as shown before (28,42), further confirming the integrity of these designed NCPs.

Binding of Pol β to single-nucleotide gaps in NCPs is significantly hindered

Although several studies had shown that the Pol β DNA gap-filling activity is significantly hindered in the NCP, quantitative assessments of Pol β and NCP interactions have not been performed. To gain a better understanding of requirements for formation of Pol β and NCP complex, we performed fluorescence anisotropy equilibrium binding assays using fluorescently tagged Pol β at mutated residue cysteine 303 (5 nM) and titrating with NCP-5′-P-THF-O (–35). This outwardly-oriented substrate mimicking an AP-incised lesion was chosen to increase the sensitivity of the assay, due to its optimal rotational orientation. Figure 2A shows a representative curve of duplicate experiments yielding a K_d value of 280 ± 100 nM. Previous equilibrium binding studies addressing the binding affinity of Pol β to free DNA containing a single nucleotide gap estimated a K_d value of ∼28 nM (43). Thus, comparison with the K_d value of the NCP suggests ∼10-fold weaker binding. For a more direct comparison of the level of inhibition on Pol β binding to the NCP, we performed a series of EMSA binding experiments, where 50 nM free DNA or NCP were incubated with varying amounts of Pol β (0–6 μM) (Figure 2B). The K_d values for DNA and NCP estimated from this assay were 20 and 360 nM, respectively. These values are in close agreement with the K_d value found in the experiment shown in Figure 2A and the previously reported K_d value for DNA. Interestingly, Figure 2C shows that the binding affinity for undamaged DNA was only minimally decreased, by ∼3-fold, compared to damage-containing DNA (K_d of 50 nM versus 20 nM, respectively). A similar decrease was observed when comparing damaged and undamaged NCPs, yielding K_d values of 360 nM versus 740 nM, respectively. In fact, the level of inhibition imposed by the histones for this damaged NCP-5′-P-THF-O (–35) and undamaged site was ∼20-fold for both substrates (Table 1). For the substrate at -35 containing a single-nucleotide gap without the 5′-dRP group [NCP-gO (–35)], containing a 5′-phosphate and 3′-OH terminus, binding of Pol β to the NCP was inhibited ∼25-fold relative to the corresponding free DNA (Supplementary Figure S2A and Table 1), suggesting the presence of the 5′-dRP group minimally influenced binding.

Previously, it was proposed that translational positioning of the single-nucleotide gaps was a stronger determinant for DNA synthesis activity relative to the effects of rotational positioning (28), due to weaker histone-DNA interactions and the increased malleability of DNA with increased distance from the dyad. To address whether the translational positioning of the substrate has an effect on binding, the binding affinity of Pol β for a nucleosomal substrate containing a single-nucleotide gap closer to the DNA end, but inwardly-oriented [NCP-gI (–49)], was determined by EMSA (Supplementary Figure S2B). These assays revealed that binding of Pol β to nucleosomal DNA was im-

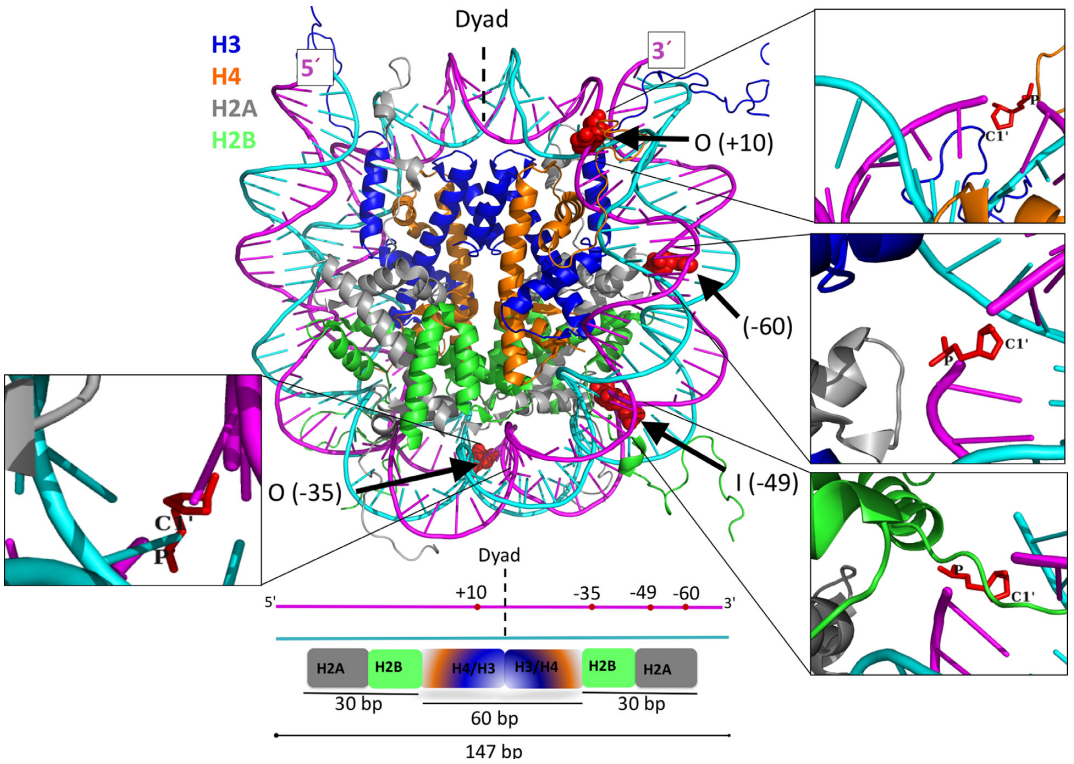

Figure 1. Structural features of designed 5′-dRP lesions and single nucleotide gaps in the nucleosome core particle (NCP). The color designation of the histones is shown at the top left and bottom. The template and lesion-containing strands of DNA are in cyan and magenta, respectively. Incorporation of dU within the nick at different locations allowed for strategic positioning of the lesions (red spheres) when reconstituted with the histone octamer so that they encompass the major structural parameters that regulate BER in the NCP: rotational and translational positioning of the DNA lesion. A total of four substrates containing either a 5′-dRP group or a single-nucleotide gap were used in this study: two outwardly oriented O (+10) and O (–35), one inwardly oriented I (–49), and a lesion with no definitive rotational orientation located only 13 nt from the DNA ends (–60). As shown in the diagram at the bottom, the central 60 bp are organized by the histone H3–H4 tetramer; whereas, the 30 nt on either side are in contact with the H2A-H2B heterodimer, and the remaining 13 nt are loosely associated with the histones. The difference in histone–DNA interactions in the central region vs. the ends gives rise to intrinsic differences in accessibility where regions bound by the H2B–H2A heterodimers are intrinsically more dynamic as described by others (47).

Table 1. Apparent dissociation constants of Pol β for DNA and NCP substrates

Substrate	K_d (nM)	Ratio (DNA/NCP)
UND-DNA	50 ± 20	
UND NCP	740 ± 70	0.06 ± 0.02
DNA-gO (-35)	20 ± 4	
NCP-gO (-35)	460 ± 40	0.04 ± 0.005
DNA-5′-P-THF-O (-35)	20 ± 2	
NCP-5′-P-THF-O (-35)	360 ± 40	0.06 ± 0.0002
DNA-gI (-49)	30 ± 8	
NCP-gI (-49)	170 ± 20	0.18 ± 0.02

Pol β binding to DNA is largely non-specific at 37 mM KCl, where the presence of the histone octamer significantly hinders this interactions by 6-fold to 25-fold depending on the structural location of the lesion. These data represent the mean of three independent experiments ± SD. The binding curves are shown in Figure 2 and Supplementary Figure S2.

proved ∼3-fold in the presence of a single-nucleotide gap 24 bp from the DNA end as compared to 38 bp from the end. DNA breathing may be sufficient to expose DNA gaps and improve binding, although DNA synthesis would still necessitate significant distortion on the templating strand with stable interactions on both strands mediated by the 31-kDa domain. Taken together, these data suggest that the histone octamer strongly dictates binding, independent of DNA damage, and Pol β binding to NCPs is largely driven by non-specific interactions.

Pol β 5′-dRP lyase reaction proceeds unperturbed in NCPs

We compared kinetic parameters of Pol β 5′-dRP group removal from free DNA and NCPs. A representative phosphor image of a denaturing gel is shown at the bottom of Figure 3A. The appearance of a faster migrating band with incubation time, relative to the no enzyme control (-E), illustrates the enzymatic activity. Importantly, the negative control without Pol β shows some spontaneous loss of the dRP group in free DNA as expected due to the heat-labile nature of the 5′-dRP group (44). However, slightly more sponta-

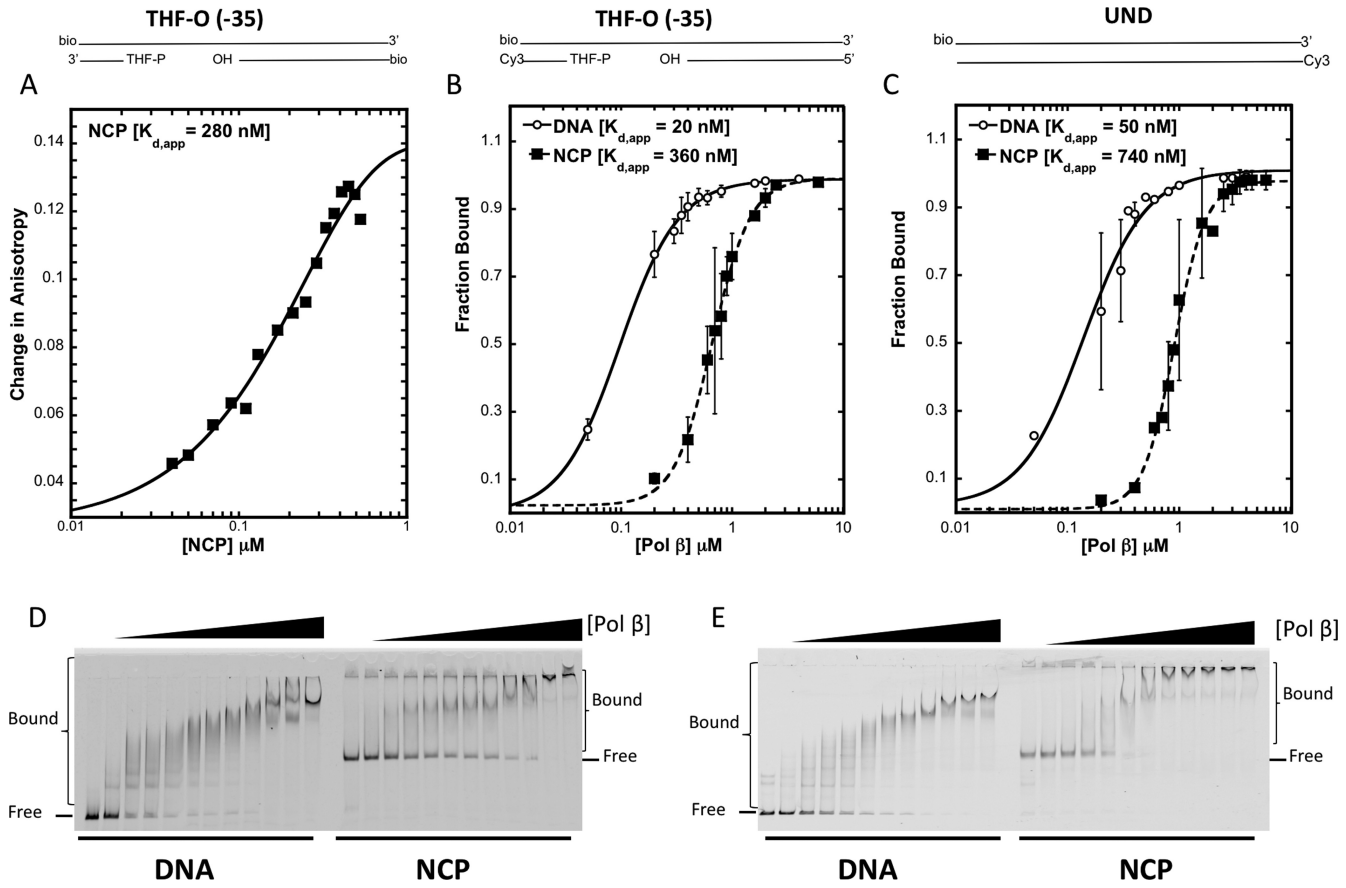

Figure 2. Pol β binding to damaged and undamaged DNA and NCPs**.** Schematic representations of substrates are illustrated on top of each panel. (**A**) Fluorescently labeled Pol β V303C (5 nM) was titrated with NCPs containing 5′-phosphorylated tetrahydrofuran (5′-P-THF) at the 5′-end of a DNA nick located 35 nucleotides from the dyad [NCP-5′-P-THF-O (–35)] mimicking a single-nucleotide gap with a stable 5′-dRP group. The 5′-ends were blocked with biotin (bio) to prevent binding of Pol β to 5′-phosphates. A representative curve from duplicate anisotropy experiments is shown. (**B**) DNA and NCP substrates containing 5′-P-THF at position -35 were incubated with 0–6 μM of Pol β on ice for 10 min. A representative image of a non-denaturing 6% polyacrylamide gel is shown in panel (**D**). (**C**) Undamaged (UND) DNA and NCP substrates were similarly incubated with varying amounts of Pol β as described in (**B**) with a representative image of a non-denaturing 6% polyacrylamide gel shown in (**E**). The data points and error bars shown in panels B & C represent the mean of three independent experiments ± SD. The solid line corresponds to the fits of the data as described in Materials and Methods using a modified Hill binding equation from which the apparent dissociation constants were derived (Table 1).

neous loss of the 5′-dRP group was observed in the NCP. This is likely due to the basic environment provided by the histones. Unlike any other site, Pol β catalyzed dRP removal was enhanced at NCP-dRP (-60) by ∼16 fold as compared to free DNA (Figure 3B and Table 2). Similarly removal of the dRP group at -60 by the 8-kDa domain of Pol β was enhanced ∼3-fold over free DNA (Figure 3B and Table 3). Because the spontaneous background loss was subtracted, the enhanced Pol β activity was not due to background dRP release. Independent experiments for this site, with 3′-end labeled substrate confirmed this enhancement of Pol β activity on the NCP relative to free DNA (Supplementary Figure S3). However, these rates with 3′-end labeled substrate were faster, likely due to the suboptimal separation of $\frac{1}{2}$ nucleotide faster migrating product relative to the substrate band (Supplementary Figure S3A). Because the 5′-end label assay allows for better separation between the substrate and product, all dRP reactions were performed with the 5′-end label assay.

Pol β catalyzed dRP removal at nucleosomal sites –35 and –49 with similar activity as free DNA (Figure 4A, B, Table 2). NCP-dRP-O (+10), close to the dyad, exhibited a ∼2-fold higher activity relative to free DNA (Table 2). Relative to their respective free DNAs, removal of the 5′-dRP group in NCPs by the 8-kDa domain of Pol β was inhibited 3-fold and 4-fold at NCP-dRP-I (–49) and NCP-dRP-O (–35), respectively (Figure 4A and B and Table 3), indicating that DNA contacts mediated by the missing 31-kDa domain are important for removal of 5′-dRP lesions, where the DNA gap is well positioned and occluded. Importantly, mutation of Lysine residues to Alanine located in the active site of the 8-kDa domain (K35A, K68A and K72A) decreased 5′- dRP removal at NCP-dRP-O (–35) where no significant product formation was detected at 360 s (Supplementary Figure S5), suggesting that the observed dRP elimination is Pol β catalyzed (33). Taken together, these results show that the NCP fails to impose constraints to Pol β catalyzed 5′-dRP removal, and in fact, the NCP enhances the rate of 5′-dRP removal at specific sites.

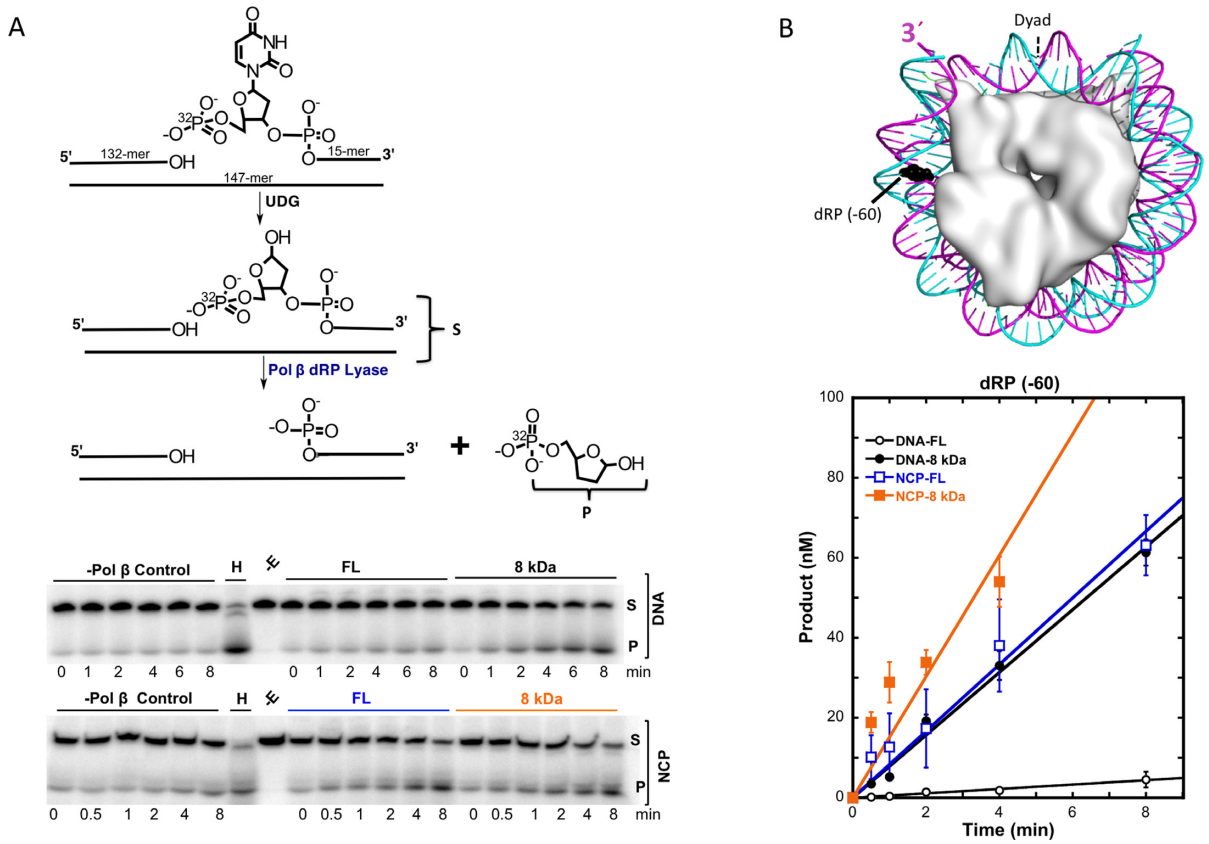

Figure 3. Pol β dRP lyase activity assay. (**A**) DNA oligo (15-mer) was 5′-end labeled with γ-^{32}P-ATP. Experiments were conducted as described in Materials and Methods. The reaction with Pol β was initiated ∼30 s after UDG incubation. A negative control was included to subtract the spontaneous loss of the 5′-dRP. A heat control (H), as described in Materials and Methods, was included to determine the actual dRP substrate generated after the 5.5-min UDG incubation. Full length Pol β (FL) or the N-terminal domain of Pol β (8 kDa) were used to determine dRP lyase activity. A representative phosphor image of a 20% polyacrylamide denaturing gel of the replicates plotted in panel (B) is shown. (**B**) NCP crystal structure pdb file 3LZ0 (37) was modified to show the structural location of the 5′-dRP group (black spheres). This is the back view of that shown in Figure 1. Data represent the mean of three independent experiments ± SD. Kinetic parameters are provided in Table 2 (full length Pol β) and Table 3 (8 kDa domain of Pol β). As shown in Table 2, the ratio (DNA/NCP) of the enzymatic rates for this 5′-end labeled substrate is comparable to the ratio found by the 3′-end labeling assay (Supplementary Figure S3). The rate of spontaneous loss, estimated from the –Pol β control, for the NCP is ∼3.2 nM/min, which is 8-fold faster than the rate in DNA of 0.4 nM/min.

Table 2. Kinetic parameters for 5′-dRP removal by Pol β in DNA and NCPs

Substrate	k_{app} (min^{-1})	Ratio (DNA/NCP)
DNA-dRP-O (+10)	0.009 ± 0.001	
NCP-dRP-O (+10)	0.021 ± 0.004	0.43 ± 0.03
DNA-dRP-O (-35)	0.21 ± 0.01	
NCP-dRP-O (-35)	0.28 ± 0.003	0.75 ± 0.03
DNA-dRP-I (-49)	0.09 ± 0.002	
NCP-dRP-I (-49)	0.07 ± 0.004	1.3 ± 0.04
DNA-dRP (-60)	0.01 ± 0.001	
NCP-dRP (-60)	0.16 ± 0.01	0.06 ± 0.002

Data represent the average of three independent experiments ± SD with the error in the ratio calculated using standard propagation of error with standard deviation procedures. Data correspond to plots shown in Figures 3B and 4 and are expressed as initial rate/enzyme concentration.

Pol β catalyzed nucleotide insertion is strongly inhibited by the NCP in a manner consistent with site exposure and DNA flexibility

Several groups have assessed gap-filling activity of Pol β in NCPs, and while some have found reduced gap-filling activity in NCPs (28–31,45), others have reported complete inhibition of DNA synthesis in NCPs (19,32). These differences are likely attributed to a combination of DNA sequence, size of the nucleotide gap, structural position of the lesions, and assay conditions. As evident from these studies, it is clear that the histone octamer poses a significant barrier to the gap-filling activity of Pol β; however, the extent of this inhibition is still imprecise particularly as it relates to structural positioning. Determination of kinetic parameters, which have not been performed for these sites, is necessary to help uncover the factors contributing to the inhi-

Table 3. Kinetic parameters for 5′-dRP removal by the 8 kDa domain of Pol β in free DNA and NCPs

Substrate	k_{app} (min^{-1})	Ratio (DNA/NCP)
DNA-dRP-O (+10)	0.015 ± 0.002	
NCP-dRP-O (+10)	0.016 ± 0.001	0.94 ± 0.07
DNA-dRP-O (-35)	0.24 ± 0.01	
NCP-dRP-O (-35)	0.06 ± 0.005	4.0 ± 0.17
DNA-dRP-I (-49)	0.02 ± 0.001	
NCP-dRP-I (-49)	0.006 ± 0.005	3.3 ± 0.11
DNA-dRP (-60)	0.05 ± 0.002	
NCP-dRP (-60)	0.14 ± 0.01	0.36 ± 0.02

Data represent the average of three independent experiments ± SD for all except for dRP-O (+10), which were performed in duplicates for DNA and NCP, in which case the error in the fit is shown. Data correspond to plots shown in Figures 3B and 4 and are expressed as initial rate/enzyme concentration.

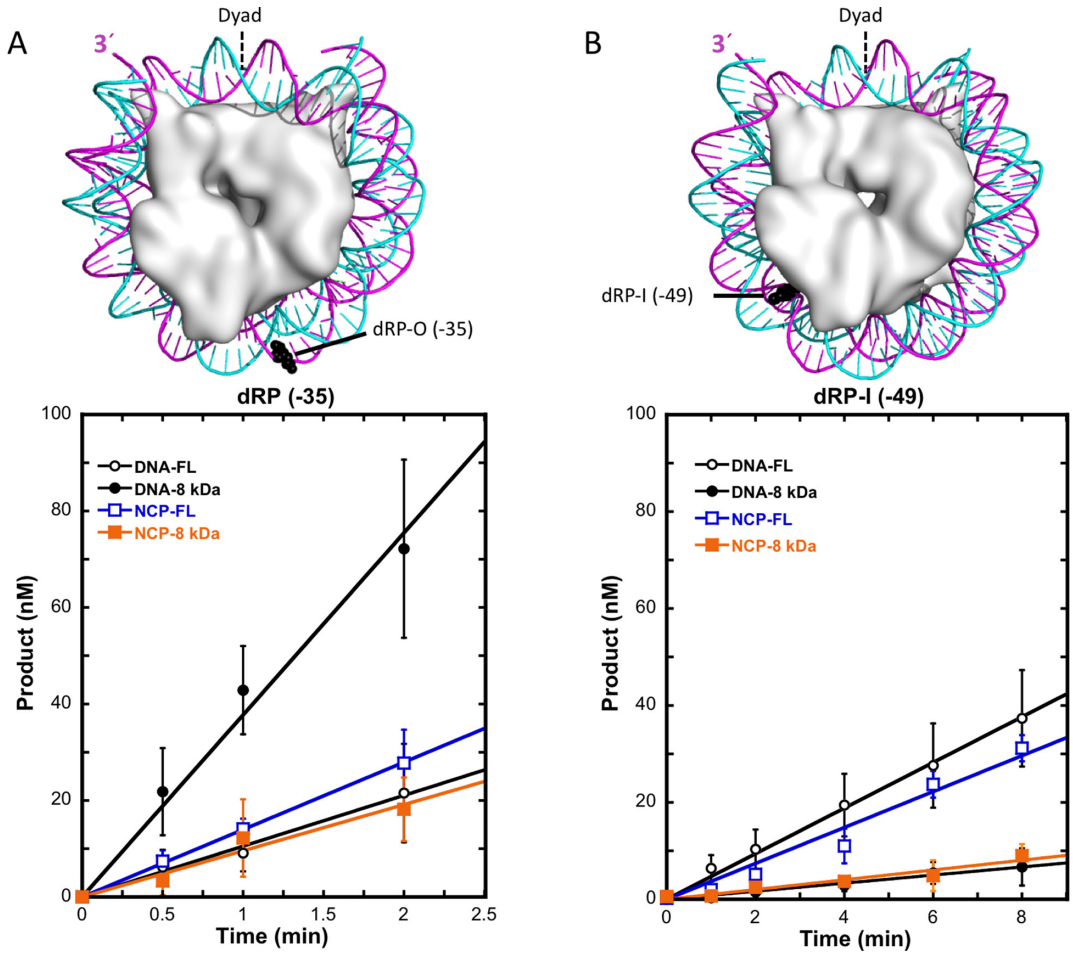

Figure 4. Pol β dRP lyase activity on inwardly- and outwardly-oriented 5′-dRP intermediate near the DNA ends. The procedure presented in Figure 3A was employed for these experiments. The crystal structure pdb file 3LZ0 was modified to show the structural location of the 5′-dRP group (black spheres) in (**A**) dRP-O (–35) and in (**B**) dRP-I (–49). Experiments were conducted as described in Materials and Methods. The data represent the mean of three independent experiments ± SD. Comparisons of the kinetic parameters are shown in Tables 2 and 3. The rate of spontaneous loss, estimated from the –Pol β control, was the same in free DNA and corresponding NCP substrate with 1.4 nM/min for dRP-O (–35) and 0.4 nM/min for dRP-I (–49).

bition. This is particularly important for the current study given that we observed efficient and even enhanced activity with 5′-dRP groups in NCPs.

To determine nucleotide insertion by Pol β, single-nucleotide gaps were generated by incubating uracil-containing nicked ^{32}P 5′-end labeled DNA substrates with UDG (Figure 5A) followed by assembly of NCPs. Figure 5B summarizes the location of the single-nucleotide gap substrates within the NCPs. DNA gap-filling was assessed by the appearance of a 1-nt slower migrating band (P) relative to the untreated control (S) as shown in Figure 5C. Single turnover experiments revealed a very strong inhibition, ∼ 2600-fold, near the dyad [(NCP-gO (+10)] as compared to free DNA (Figure 5D and Table 4). This may be indicative of constraints on required conformational changes in the substrate or enzyme for catalysis. The occlusion of the

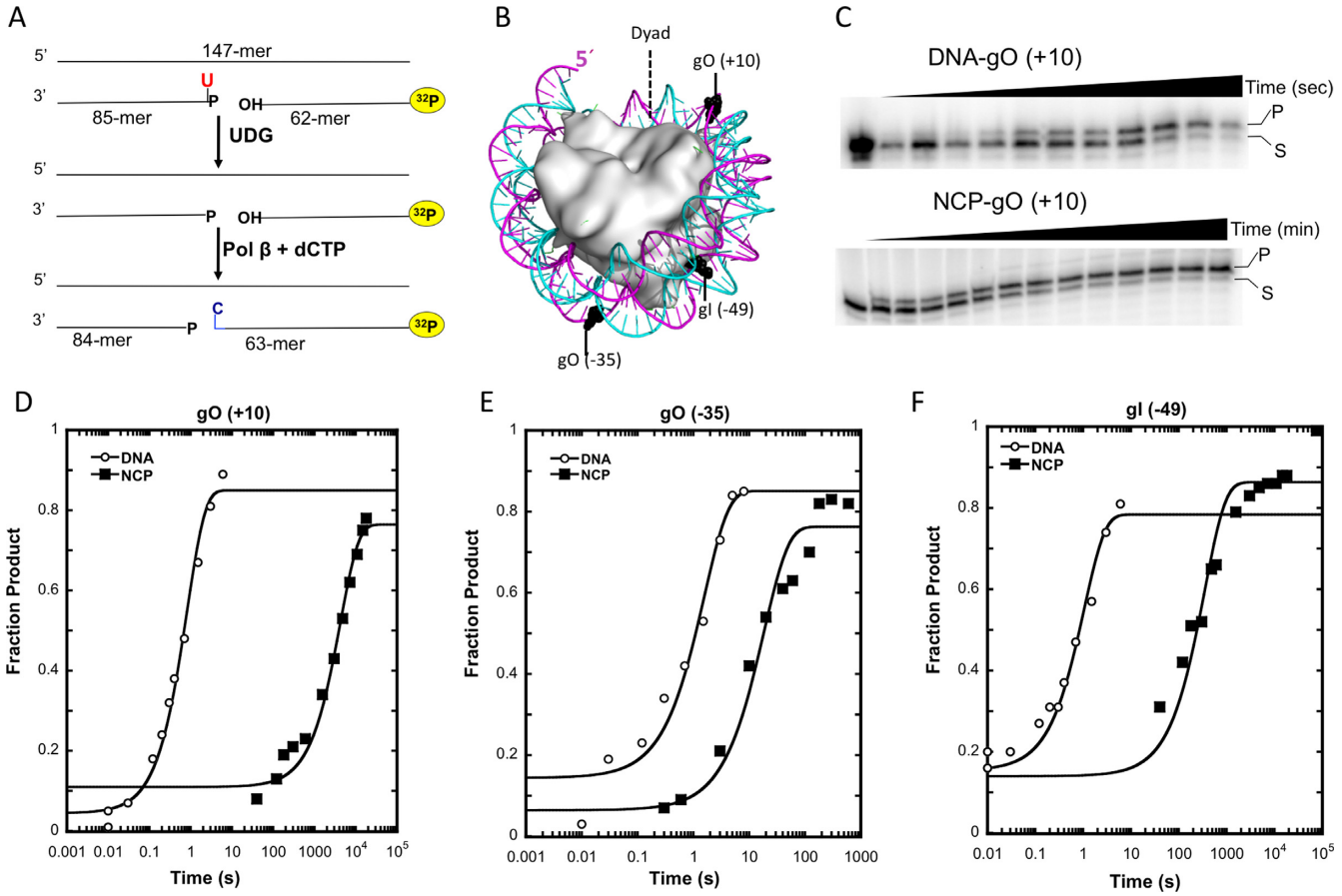

Figure 5. The effect of rotational and translational positioning of a single-nucleotide gap on the single-turnover kinetics of Pol β catalyzed nucleotide insertion in NCPs. (**A**) Schematic illustrating the generation of the substrate and determination of the product by the appearance of 1-nt slower migrating band for gO (+10) substrates. (**B**) Structural location of the single-nucleotide gaps (black spheres). (**C**) Representative phosphor image of an 8% denaturing polyacrylamide sequencing gel for DNA-gO (+10) and NCP-gO (+10) showing the appearance of the product (P) as 1-nt slower migrating band relative to the substrate (S). Representative plots of three independent experiments are shown: (D) gO (+10), (**E**) gO (–35) and (**F**) gI (–49). The time- course for DNA was from 0–8 s and for NCP from 0–190 min. The final concentration for all single turnover experiments was 10 nM DNA, or 100 nM NCP with 1 μM Pol β and 50 μM dNTP. Data analysis and kinetic fits are described in Materials and Methods, and average rate constants from three independent experiments are summarized in Table 4.

single-nucleotide gap by the histone octamer at NCP-gI (–49), resulted in inhibition (∼277-fold) (Figure 5F and Table 4), suggesting the rotational orientation of the single-nucleotide gap plays a strong role in blocking gap-filling by Pol β. Thus, DNA breathing in this region is not sufficient to allow full accessibility to the DNA gap. A similar level of inhibition, but 3-fold lower, was observed at NCP-g (–60) (Supplementary Figure S6 and Table 4).

Steady-state measurements showed DNA-gap filling activity was inhibited 8-fold near the DNA ends at NCP-g (–60) (Figure 6A). For another single-nucleotide gap at NCP-gO (+10), the inhibition was significantly greater (178-fold) (Figure 6B) relative to free DNA. The level of inhibition observed in the steady-state assay for these lesions was much lower than the level of inhibition observed under single turnover conditions. This was because the rate-limiting step for Pol β turnover with free DNA is product release, and this was slower than the insertion rate measured under single-turnover conditions. These results are in agreement with previous findings proposing that the translational positioning of single-nucleotide gaps in NCPs plays a role in inhibiting gap-filling activity measured under steady-state conditions (28). However, the effect of rotational orientation near the DNA ends was previously underestimated (28). In the current study, we show that despite the enhancement of 5′-dRP group removal at –60, DNA synthesis at this site is inhibited.

DISCUSSION

Given the critical role that dRP lyase activity plays *in vivo* and the biological significance of nucleosomal substrates, for the first time, we have characterized dRP removal in designed NCPs containing rotationally and translationally positioned 5′-dRP lesions. Unlike any other study that has addressed Pol β gap-filling activity in NCPs, we first determined the binding affinity of Pol β for nucleosomes and free DNA. Our results show that binding of Pol β to DNA is driven by non-specific interactions independent of DNA damage, and the presence of the histone octamer constitutes a strong barrier for Pol β.

Table 4. Single turnover catalytic rate constants for Pol β catalyzed nucleotide insertion in free DNA and NCPs

Substrate	k_{obs} (s^{-1})	Ratio (DNA/NCP)
DNA-gO (+10)	1.24 ± 0.007	
NCP-gO (+10)	0.0005 ± 0.0002	2599.6 ± 1161
DNA-gO (-35)	0.76 ± 0.07	
NCP-gO (-35)	0.18 ± 0.07	4.3 ± 1.3
DNA-gI (-49)	0.83 ± 0.17	
NCP-gI (-49)	0.003 ± 0.001	276.7 ± 36.6
DNA-g (-60)	5.4 ± 1.1	
NCP-g (-60)	0.06 ± 0.008	90.4 ± 6.4

Data represent the mean of three independent experiments ± SD and correspond to data shown in Figure 5 and Figure Supplementary S6.

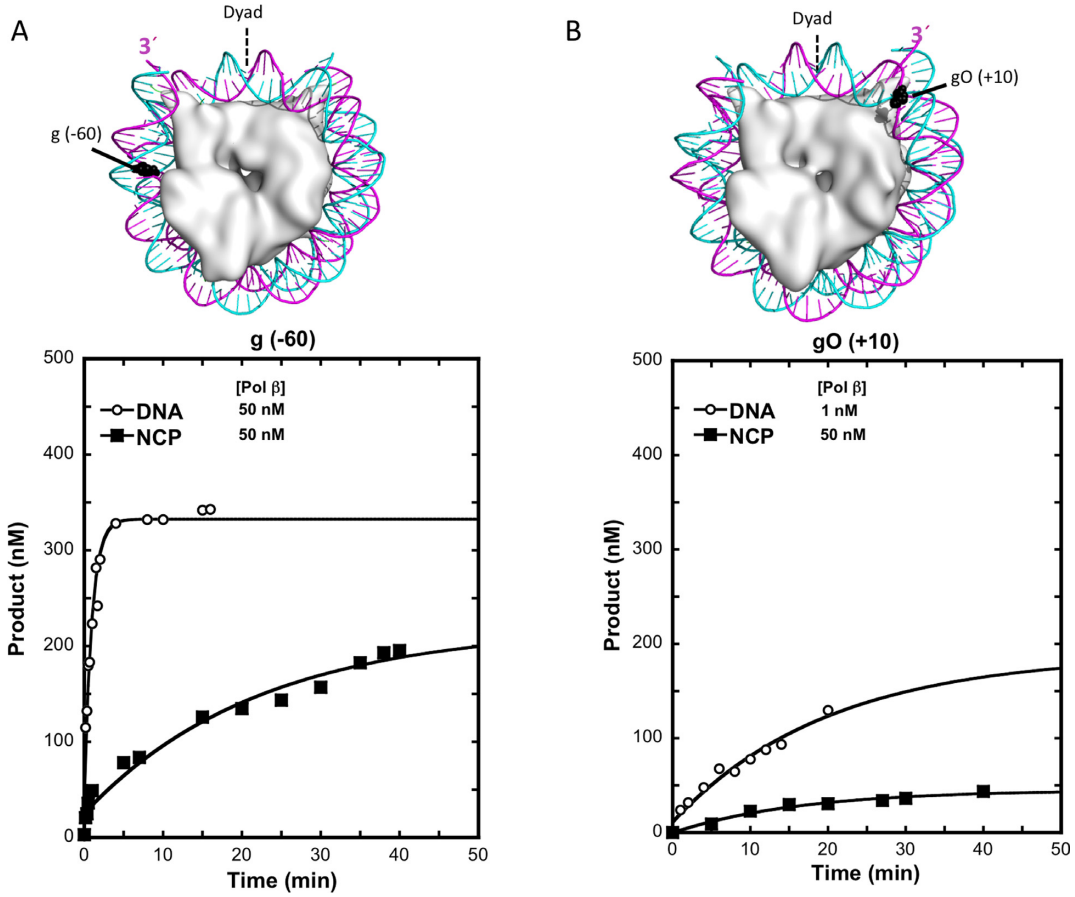

Figure 6. Steady-state kinetic analysis of Pol β catalyzed nucleotide insertion. The crystal structure of the 601 NCP pdb file 3LZ0 (37) was modified to highlight the position of the 1nt gap containing NCP substrates (black spheres). (**A**) Representative time-course for Pol β catalyzed nucleotide insertion with NCP-g (-60) and corresponding DNA. A substrate concentration of 500 nM and 50 nM Pol β for both NCP-g (–60) and DNA-g (–60) were used with 50 μM dNTP. The average rate constant from three independent experiments is 0.6 ± 0.12 min^{-1} and 4.8 ± 0.21 min^{-1} for NCP and DNA, respectively. This shows an 8-fold inhibition at NCP-g (-60). B) Representative time-course for Pol β catalyzed nucleotide insertion with NCP-gO (+10) and corresponding DNA. Final substrate concentration of DNA-gO (+10) and NCP-gO (+10) was 500 nM with 1 nM and 50 nM Pol β, respectively, and 50 μM dNTP. Rate constants derived from the kinetic fits were 0.05 ± 0.004 min^{-1} for NCP-gO (+10) compared to 8.9 ± 0.8 min^{-1} for DNA-gO (+10), illustrating a 178-fold inhibition. Data were analyzed and fitted as described in Materials and Methods.

With regards to dRP lyase activity, our results show that Pol β is able to remove the 5′-dRP group from the BER intermediates with similar efficiency as that with free DNA. In fact, 5′-dRP removal was enhanced by 16-fold near the ends at –60 [NCP-dRP (–60)] as compared to the corresponding free DNA. Although this enhancement is independent of the spontaneous 5′-dRP loss, a synergistic effect due to histone Lysines and Pol β cannot be ruled out at this site. Unlike any other site, NCP-dRP (–60) also exhibited ∼8-fold greater spontaneous loss compared to the spontaneous loss on its corresponding DNA. Inspection of the NCP crystal structure (PDB 1KX5) revealed that a single Lysine residue (histone H2AK75) is found within 8 Å of the C1′ of this lesion. The other NCP sites (+10 and –49) also are within 8 Å of Lysines H4K5 and H2BK28, respectively, but no increase in the spontaneous elimination was observed at these sites. Importantly, this distance is outside the expected catalytic distance of 3 Å. The increased spontaneous elimination ob-

served at site -60 may be due to the increased DNA dynamics and DNA flexibility at this site, which may increase the proximity of the reactive groups. The activities for 5′-dRP removal in free DNA at this site and at DNA-dRP-O (+10) were lower than the other two sites. Such differences in activity for DNA substrates have also been well documented for other BER enzymes (46). These differences are likely attributed to the inherent structural features that the DNA sequence generates on DNA shape, along with the site-specific effect of introducing a DNA nick at different locations, on the overall persistence curvature of the DNA.

The removal of the 5′-dRP group at NCP-dRP (–60) by the 8-kDa domain of Pol β was 3-fold faster relative to free DNA. Wrapping of the DNA on the surface of the histone octamer induces significant distortions on the overall helical structure of DNA, and this may provide unique site-specific structural features at this site. Because the 5′-dRP group is likely frayed, this site may orient the 5′-dRP group in a manner that allows Lys72 to more efficiently form the Schiff-base intermediate with its C1′of the ribose ring. Crystallographic studies of Pol β have revealed the enzyme and 5′-dRP group must be flexible enough to allow for optimal repositioning to the ϵ-NH_2 group of Lys72 in the lyase active site. Additionally, the weaker histone-DNA interactions near -60 may serve as a platform that facilitate additional interactions with regions flanking the 5′-dRP group promoting the enzymatic activity (47). Because this site inhibits DNA synthesis under steady-state and single turnover conditions, these local structural features appearing to enhance dRP lyase activity do not influence DNA synthesis. The activity of the 8-kDa domain of Pol β was decreased at two other NCP sites, and this was independent of rotational orientation suggesting contacts between the two Pol β domains are important at these sites for dRP removal.

DNA synthesis appears to be regulated by additional structural features of the NCP and to a much *greater* extent than dRP removal. Catalytic rates for NCPs from single turnover experiments exhibited a broad range of inhibition ranging from ∼4-fold to 2600-fold relative to free DNA. Steady-state kinetics also revealed a significant level of inhibition, although the level of inhibition was at least one order of magnitude smaller. In all cases, the NCP poses a significant barrier for DNA-gap filling by Pol β. *In vivo,* where substrate localization is critical for Pol β catalysis, once the damage is recognized, the dRP lyase reaction may proceed. However, for DNA gap-filling, structural constraints (35,48) modulating accessibility and malleability of the substrate would have an important role. Consequently, factors that can regulate these structural constraints *in vivo* are likely to have an effect on the observed kinetics including the action of ATP-dependent remodeling factors, presence of chromatin architectural proteins, and DNA sequence as it relates to NCP stability (17).

Importantly, the DNA structure on the surface of the histone octamer exhibits remarkable differences compared to the structure of free DNA. In the NCP, the DNA trajectory accommodates DNA base-pair-step geometry with twice the curvature including ∼10 bp periodicity with narrowing of minor grooves where the DNA contacts arginine residues (49). These structural features can be important for DNA repair protein read outs (50). In fact, minor groove width was postulated to be an important factor in predicting uracil reactivity in the NCP, where widening of the minor groove at two sites resulted in equal or increased reactivity compared to free DNA (25). Similarly, a 5-nt DNA flap outwardly oriented was removed 7-fold faster by FEN1 in the NCP compared to its removal in free DNA (27). Together these results suggest that local structural features relating to DNA shape and flexibility influence DNA repair by various BER proteins, highlighting the complexity of the mechanisms that regulate repair in NCPs.

Figure 7 summarizes the findings for dRP removal and DNA synthesis in NCPs in this study, as well as proposed mechanisms for the observations. We propose that in the NCP, Pol β is not able to make stable interactions with nucleosomal DNA due to steric constraints on the strand facing the histones due to its high rigidity (Figure 7A). Consequently DNA synthesis is strongly inhibited. Because the 5′-dRP lyase reaction does not require extensive interactions with the substrate-containing strand, exposure and minimal constraints on the outwardly-oriented lesions allows for dRP removal. Rotational flexibility of the DNA on the surface of the histone octamer, although minimal, allows some DNA synthesis near the dyad involving transient engagement of the 31-kDa domain. Near the DNA ends, the DNA is more accessible and consequently both enzymatic reactions take place with fewer structural constraints. Because DNA synthesis by Pol β requires far more extensive interactions and distortions on the templating strand, these requirements are not easily accommodated near the dyad due to the stronger histone-DNA interactions (Figure 7A) (47). Pol β's DNA synthesis activity in NCP is largely influenced by translational positioning of the DNA gap, suggesting that repositioning of the histone octamer may be sufficient to allow some level of gap-filling, particularly for lesions near the DNA ends. Complete eviction of the histone octamer by ATP-dependent remodeling factors may be necessary for synthesis at sites located near the dyad.

There are several biological implications for the observed differences in enzymatic activities of Pol β in the context of the NCP. The lack of parallel activities for the dual enzymatic functions of Pol β is potentially a feature evolved to induce tighter control on the lifetime of BER intermediates containing the 5′-dRP group. Persistence of the 5′-dRP group in NCPs could lead to more complex DNA repair transactions, ultimately leading to more cytotoxic effects than the initial base modification. For example, if dRP removal were inhibited or inefficient in NCPs, the increased half-life of the dRP lesion may lead to its oxidation by ROS or other chemical modifications, shifting subpathway choice from short-patch to long-patch BER. In fact, it was recently shown that DNA lesions in NCPs, using cell-free extracts or purified enzymes, are preferentially repaired by Pol β via short-patch BER (51). The dRP-lyase activity of Pol β is critical in controlling DNA repair initiated by monofunctional glycosylases as overwhelming the repair system by exposure to alkylating agents, in the absence of dRP lyase activity, leads to cell death (13).

Importantly, accumulation of these APE1 incised BER intermediates may signal recruitment of PARP1 (52), the outcome of which is likely to be dependent on the presence

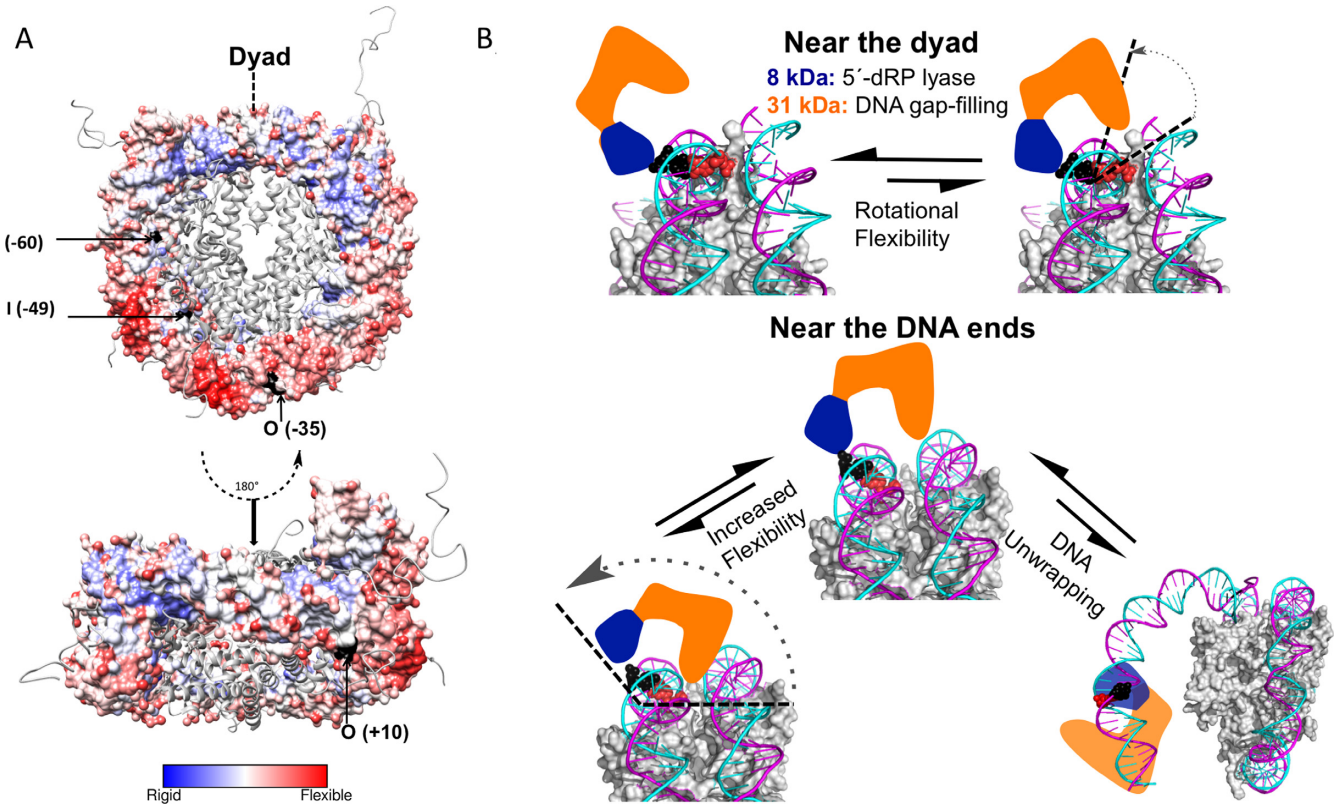

Figure 7. Model for modulation of Polymerase β enzymatic activities by the structural constraints of the nucleosome core particle. (**A**) The structure of the NCP pdb file 1KX5 was modified to display b-factor values, color-coded as blue (rigid) and red (flexible).The bottom figure is a top view of the top figure rotated 180° counter clockwise. Lesions are shown in black. (**B**) Near the dyad, outwardly oriented 5′-dRP lesions (black spheres) are repaired efficiently by Pol β; however, DNA synthesis is strongly inhibited despite the DNA gap being outwardly-oriented. This is due to occlusion of the templating base (red spheres) and the inability to stably engage the 31-kDa domain in a rigid region as shown in (A). Some DNA synthesis near the dyad occurs due to rotational flexibility, where the DNA rotates along its longitudinal axis on the surface of the histone octamer (dashed black lines). Near the DNA ends, 5′-dRP groups are repaired efficiently, and inhibition of DNA synthesis is overall decreased. This is due to increased DNA flexibility and DNA unwrapping, although DNA gap-filling is nonetheless inhibited in a site-specific manner, indicating that local structural features as well as rotational orientation of the lesion play an important role for DNA gap-filling by Pol β. Together, these results indicate external factors capable of remodeling the NCP structure are needed for efficient DNA synthesis.

or absence of the 5′-dRP lesion (53). In the absence of the 5′-dRP lesion, assuming Pol β's recruitment and dRP lyase activity occurs very rapidly, specific histone sites that are targets for posttranslational modifications may undergo activation and become PARylated by PARP1 (54). This may promote local dissociation of the histone octamer from the DNA and allow Pol β to more stably bind and perform template-directed DNA synthesis at these sites (42). In fact, retention of PARP1 at sites of DNA damage, as observed by laser-induced irradiation techniques, coincides with Pol β DNA recruitment (55). In the presence of the 5′-dRP lesion, however, PARP1 may become covalently crosslinked to this intermediate (53). DNA-protein crosslinks (DPCs), if not removed before the next round of replication, can become lethal due to replication fork stalling and/or collapse that results in double strand breaks (53).

Because several DNA glycosylases, APE1, and the lyase domain of Pol β are able to process their respective outwardly-oriented lesions, inefficient DNA gap-filling at these sites would lead to the accumulation of single-nucleotide gaps. The strongest inhibition of Pol β catalyzed DNA synthesis is near the dyad, suggesting that this region may be a hot spot for DNA mutations, if not repaired before replication. This is in agreement with recent findings that suggest mutation rate increases with nucleosome occupancy in repair proficient systems; whereas, this correlation is abolished in DNA repair knockouts (56). These results are consistent with the mutation rate being associated with decreased repair of aborted intermediates due to decreased accessibility to DNA repair proteins in NCPs, particularly at the dyad. Because of this increased mutagenic potential near the dyad, it is possible that specialized mechanisms specifically target these regions for efficient repair. One such mechanism may involve the recruitment of ATP-dependent remodeling factors. Remodels the Structure of Chromatin (RSC) has been shown to interact with NCPs at the dyad by cryoEM and by mapping the DNase footprint generated from nucleosomes bound to RSC (57,58). In yeast, RSC-mediated chromatin remodeling promotes efficient BER by enhancing DNA accessibility to BER enzymes (59). Depletion of its ATPase subunit, STH1, led to enhanced sensitivity to alkylating agent-induced DNA damage and significant inhibition of BER, in agreement with a concomitant decrease in micrococcal nuclease digestion (59). *In vitro,* the

remodeling activity of dinucleosomes by RSC in concert with the action of the histone chaperone NAP1 was required for complete repair of 8-oxo-G located in the nucleosome core (60). Other ATP-dependent chromatin remodeling factors have enhanced BER *in vitro* (61), highlighting the need for additional factors capable of changing the chromatin landscape for efficient repair.

In addition to the involvement of ATP-dependent chromatin remodeling complexes evicting or repositioning histone octamer complexes along the DNA, intrinsic mechanisms regulating DNA accessibility in the chromatin architecture exist. DNA sequence, for example, plays a crucial role in nucleosome core particle stability *in vivo* (17,62) and *in vitro* (63). Accessibility of DNA sites within nucleosomes can be largely influenced by the DNA's relative binding affinity for the histone octamer during repair (64). Natural DNA sequences exhibit a wide range of binding affinities, varying by as much as 5000-fold (65). The 601-DNA sequence used in this study is representative of well-positioned nucleosomes *in vivo*. This suggests that even the most strongly positioned NCPs would undergo 5′-dRP removal unassisted, while more weakly positioned NCPs *may* exhibit greater gap-filling activity. However, qualitative studies using designed nucleosome core particles containing weaker DNA positioning sequences (relative to the 601) suggest gap-filling activity by Pol β is nonetheless inhibited (19,29,30). Additionally NCP stability is also regulated by histone octamer composition (26), which adds an additional level of complexity to our understating of BER in chromatin, as it constitutes a largely underinvestigated topic in the field.

It is evident from our study that the regulation of Pol β's enzymatic activities by the structure of the nucleosome core particle potentially entails a number of interconnected intrinsic mechanisms that extend beyond rotational and translational positioning of the lesion. Consequently, it is of importance to understand the nature of the molecular interactions of Pol β with nucleosomal substrates to assign parameters responsible for the observations described here.

SUPPLEMENTARY DATA

Supplementary Data are available at NAR Online.

ACKNOWLEDGEMENTS

We thank the Wilson lab members for feedback on this manuscript with special thanks to David Shock for technical advice and William Beard for helping identify important structural features near the lesions. We thank Natalie Gassman for the V303C construct of Pol β and Esther Hou for purifying the recombinant histone proteins.

FUNDING

Intramural Research Program of the National Institutes of Health, National Institute of Environmental Health Sciences [Z01ES050158 and Z01ES050159]. Funding for open access charge: Intramural Research Program of the National Institutes of Health, National Institute of Environmental Health Sciences [Z01ES050158 and Z01ES050159].

Conflict of interest statement. None declared.

REFERENCES

1. Lindahl,T. (1993) Instability and decay of the primary structure of DNA. *Nature*, **362**, 709–715.
2. Hoeijmakers,J.H. (2001) Genome maintenance mechanisms for preventing cancer. *Nature*, **411**, 366–374.
3. Baute,J. and Depicker,A. (2008) Base excision repair and its role in maintaining genome stability. *Crit. Rev. Biochem. Mol. Biol.*, **43**, 239–276.
4. Schermerhorn,K.M. and Delaney,S. (2014) A chemical and kinetic perspective on base excision repair of DNA. *Acc. Chem. Res.*, **47**, 1238–1246.
5. Beard,W.A., Prasad,R. and Wilson,S.H. (2006) Activities and mechanism of DNA polymerase beta. *Methods Enzymol.*, **408**, 91–107.
6. Almeida,K.H. and Sobol,R.W. (2007) A unified view of base excision repair: lesion-dependent protein complexes regulated by post-translational modification. *DNA Repair (Amst.)*, **6**, 695–711.
7. Sobol,R.W., Horton,J.K., Kuhn,R., Gu,H., Singhal,R.K., Prasad,R., Rajewsky,K. and Wilson,S.H. (1996) Requirement of mammalian DNA polymerase-beta in base-excision repair. *Nature*, **379**, 183–186.
8. Matsumoto,Y. and Kim,K. (1995) Excision of deoxyribose phosphate residues by DNA polymerase beta during DNA repair. *Science*, **269**, 699–702.
9. Piersen,C.E., Prasad,R., Wilson,S.H. and Lloyd,R.S. (1996) Evidence for an imino intermediate in the DNA polymerase beta deoxyribose phosphate excision reaction. *J. Biol. Chem.*, **271**, 17811–17815.
10. Beard,W.A. and Wilson,S.H. (2006) Structure and mechanism of DNA polymerase Beta. *Chem. Rev.*, **106**, 361–382.
11. Pelletier,H., Sawaya,M.R., Kumar,A., Wilson,S.H. and Kraut,J. (1994) Structures of ternary complexes of rat DNA polymerase beta, a DNA template-primer, and ddCTP. *Science*, **264**, 1891–1903.
12. Prasad,R., Kumar,A., Widen,S.G., Casas-Finet,J.R. and Wilson,S.H. (1993) Identification of residues in the single-stranded DNA-binding site of the 8-kDa domain of rat DNA polymerase beta by UV cross-linking. *J. Biol. Chem.*, **268**, 22746–22755.
13. Sobol,R.W., Prasad,R., Evenski,A., Baker,A., Yang,X.P., Horton,J.K. and Wilson,S.H. (2000) The lyase activity of the DNA repair protein beta-polymerase protects from DNA-damage-induced cytotoxicity. *Nature*, **405**, 807–810.
14. Starcevic,D., Dalal,S. and Sweasy,J.B. (2004) Is there a link between DNA polymerase beta and cancer? *Cell Cycle*, **3**, 998–1001.
15. Luger,K. (2003) Structure and dynamic behavior of nucleosomes. *Curr. Opin. Genet. Dev.*, **13**, 127–135.
16. Jiang,C. and Pugh,B.F. (2009) Nucleosome positioning and gene regulation: advances through genomics. *Nat. Rev. Genet.*, **10**, 161–172.
17. Segal,E., Fondufe-Mittendorf,Y., Chen,L., Thastrom,A., Field,Y., Moore,I.K., Wang,J.P. and Widom,J. (2006) A genomic code for nucleosome positioning. *Nature*, **442**, 772–778.
18. Dechassa,M.L.L.K. (2011) Deutsches Krebsforschungszentrum (DKFZ). In: BioQuant,RGGOF (ed). *Organization and Function in the Cell Nucleus*. Germany.
19. Beard,B.C., Wilson,S.H. and Smerdon,M.J. (2003) Suppressed catalytic activity of base excision repair enzymes on rotationally positioned uracil in nucleosomes. *Proc. Natl. Acad. Sci. U.S.A.*, **100**, 7465–7470.
20. Cole,H.A., Tabor-Godwin,J.M. and Hayes,J.J. (2010) Uracil DNA glycosylase activity on nucleosomal DNA depends on rotational orientation of targets. *J. Biol. Chem.*, **285**, 2876–2885.
21. Hinz,J.M. (2014) Impact of abasic site orientation within nucleosomes on human APE1 endonuclease activity. *Mutat. Res.*, **766–767**, 19–24.
22. Hinz,J.M., Rodriguez,Y. and Smerdon,M.J. (2010) Rotational dynamics of DNA on the nucleosome surface markedly impact accessibility to a DNA repair enzyme. *Proc. Natl. Acad. Sci. U.S.A.*, **107**, 4646–4651.
23. Odell,I.D., Wallace,S.S. and Pederson,D.S. (2013) Rules of engagement for base excision repair in chromatin. *J. Cell Physiol.*, **228**, 258–266.
24. Prasad,A., Wallace,S.S. and Pederson,D.S. (2007) Initiation of base excision repair of oxidative lesions in nucleosomes by the human, bifunctional DNA glycosylase NTH1. *Mol. Cell Biol.*, **27**, 8442–8453.

25. Ye,Y., Stahley,M.R., Xu,J., Friedman,J.I., Sun,Y., McKnight,J.N., Gray,J.J., Bowman,G.D. and Stivers,J.T. (2012) Enzymatic excision of uracil residues in nucleosomes depends on the local DNA structure and dynamics. *Biochemistry*, **51**, 6028–6038.
26. Rodriguez,Y., Hinz,J.M. and Smerdon,M.J. (2015) Accessing DNA damage in chromatin: Preparing the chromatin landscape for base excision repair. *DNA Repair (Amst.)*, **32**, 113–119.
27. Huggins,C.F., Chafin,D.R., Aoyagi,S., Henricksen,L.A., Bambara,R.A. and Hayes,J.J. (2002) Flap endonuclease 1 efficiently cleaves base excision repair and DNA replication intermediates assembled into nucleosomes. *Mol. Cell*, **10**, 1201–1211.
28. Rodriguez,Y. and Smerdon,M.J. (2013) The structural location of DNA lesions in nucleosome core particles determines accessibility by base excision repair enzymes. *J. Biol. Chem.*, **288**, 13863–13875.
29. Nilsen,H., Lindahl,T. and Verreault,A. (2002) DNA base excision repair of uracil residues in reconstituted nucleosome core particles. *EMBO J.*, **21**, 5943–5952.
30. Odell,I.D., Barbour,J.E., Murphy,D.L., Della-Maria,J.A., Sweasy,J.B., Tomkinson,A.E., Wallace,S.S. and Pederson,D.S. (2011) Nucleosome disruption by DNA ligase III-XRCC1 promotes efficient base excision repair. *Mol. Cell. Biol.*, **31**, 4623–4632.
31. Howard,M.J., Rodriguez,Y. and Wilson,S.H. (2017) DNA polymerase beta uses its lyase domain in a processive search for DNA damage. *Nucleic Acids Res.*, **45**, 3822–3832.
32. Balliano,A., Hao,F., Njeri,C., Balakrishnan,L. and Hayes,J.J. (2017) HMGB1 Stimulates Activity of Polymerase beta on Nucleosome Substrates. *Biochemistry*, **56**, 647–656.
33. Prasad,R., Batra,V.K., Yang,X.P., Krahn,J.M., Pedersen,L.C., Beard,W.A. and Wilson,S.H. (2005) Structural insight into the DNA polymerase beta deoxyribose phosphate lyase mechanism. *DNA Repair (Amst.)*, **4**, 1347–1357.
34. Sczepanski,J.T., Wong,R.S., McKnight,J.N., Bowman,G.D. and Greenberg,M.M. (2010) Rapid DNA-protein cross-linking and strand scission by an abasic site in a nucleosome core particle. *Proc. Natl. Acad. Sci. U.S.A.*, **107**, 22475–22480.
35. Beard,W.A. and Wilson,S.H. (2014) Structure and mechanism of DNA polymerase beta. *Biochemistry*, **53**, 2768–2780.
36. Beard,W.A. and Wilson,S.H. (1995) Purification and domain-mapping of mammalian DNA polymerase beta. *Methods Enzymol.*, **262**, 98–107.
37. Vasudevan,D., Chua,E.Y. and Davey,C.A. (2010) Crystal structures of nucleosome core particles containing the '601' strong positioning sequence. *J. Mol. Biol.*, **403**, 1–10.
38. Luger,K., Mader,A.W., Richmond,R.K., Sargent,D.F. and Richmond,T.J. (1997) Crystal structure of the nucleosome core particle at 2.8 A resolution. *Nature*, **389**, 251–260.
39. Duan,M.R. and Smerdon,M.J. (2010) UV damage in DNA promotes nucleosome unwrapping. *J. Biol. Chem.*, **285**, 26295–26303.
40. Luger,K., Rechsteiner,T.J. and Richmond,T.J. (1999) Preparation of nucleosome core particle from recombinant histones. *Methods Enzymol.*, **304**, 3–19.
41. Ryder,S.P., Recht,M.I. and Williamson,J.R. (2008) Quantitative analysis of protein-RNA interactions by gel mobility shift. *Methods Mol. Biol.*, **488**, 99–115.
42. Rodriguez,Y., Hinz,J.M., Laughery,M.F., Wyrick,J.J. and Smerdon,M.J. (2016) Site-specific acetylation of histone H3 decreases polymerase beta activity on nucleosome core particles in vitro. *J. Biol. Chem.*, **291**, 11434–11445.
43. Beard,W.A., Shock,D.D. and Wilson,S.H. (2004) Influence of DNA structure on DNA polymerase beta active site function: extension of mutagenic DNA intermediates. *J. Biol. Chem.*, **279**, 31921–31929.
44. Admiraal,S.J. and O'Brien,P.J. (2017) Reactivity and cross-linking of 5′-terminal abasic sites within DNA. *Chem. Res. Toxicol.*, **30**, 1317–1326.
45. Menoni,H., Gasparutto,D., Hamiche,A., Cadet,J., Dimitrov,S., Bouvet,P. and Angelov,D. (2007) ATP-dependent chromatin remodeling is required for base excision repair in conventional but not in variant H2A.Bbd nucleosomes. *Mol. Cell. Biol.*, **27**, 5949–5956.
46. Donigan,K.A. and Sweasy,J.B. (2009) Sequence context-specific mutagenesis and base excision repair. *Mol. Carcinog.*, **48**, 362–368.
47. Tims,H.S., Gurunathan,K., Levitus,M. and Widom,J. (2011) Dynamics of nucleosome invasion by DNA binding proteins. *J. Mol. Biol.*, **411**, 430–448.
48. McGinty,R.K. and Tan,S. (2015) Nucleosome structure and function. *Chem. Rev.*, **115**, 2255–2273.
49. Richmond,T.J. and Davey,C.A. (2003) The structure of DNA in the nucleosome core. *Nature*, **423**, 145–150.
50. West,S.M., Rohs,R., Mann,R.S. and Honig,B. (2010) Electrostatic interactions between arginines and the minor groove in the nucleosome. *J. Biomol. Struct. Dyn.*, **27**, 861–866.
51. Meas,R. and Smerdon,M.J. (2016) Nucleosomes determine their own patch size in base excision repair. *Sci. Rep.*, **6**, 27122.
52. Lavrik,O.I., Prasad,R., Sobol,R.W., Horton,J.K., Ackerman,E.J. and Wilson,S.H. (2001) Photoaffinity labeling of mouse fibroblast enzymes by a base excision repair intermediate. Evidence for the role of poly(ADP-ribose) polymerase-1 in DNA repair. *J. Biol. Chem.*, **276**, 25541–25548.
53. Prasad,R., Horton,J.K., Chastain,P.D. 2nd, Gassman,N.R., Freudenthal,B.D., Hou,E.W. and Wilson,S.H. (2014) Suicidal cross-linking of PARP-1 to AP site intermediates in cells undergoing base excision repair. *Nucleic Acids Res.*, **42**, 6337–6351.
54. Messner,S., Altmeyer,M., Zhao,H., Pozivil,A., Roschitzki,B., Gehrig,P., Rutishauser,D., Huang,D., Caflisch,A. and Hottiger,M.O. (2010) PARP1 ADP-ribosylates lysine residues of the core histone tails. *Nucleic Acids Res.*, **38**, 6350–6362.
55. Gassman,N.R. and Wilson,S.H. (2015) Micro-irradiation tools to visualize base excision repair and single-strand break repair. *DNA Repair (Amst.)*, **31**, 52–63.
56. Yazdi,P.G., Pedersen,B.A., Taylor,J.F., Khattab,O.S., Chen,Y.H., Chen,Y., Jacobsen,S.E. and Wang,P.H. (2015) Increasing nucleosome occupancy is correlated with an increasing mutation rate so long as DNA repair machinery is intact. *PLoS One*, **10**, e0136574.
57. Chaban,Y., Ezeokonkwo,C., Chung,W.H., Zhang,F., Kornberg,R.D., Maier-Davis,B., Lorch,Y. and Asturias,F.J. (2008) Structure of a RSC-nucleosome complex and insights into chromatin remodeling. *Nat. Struct. Mol. Biol.*, **15**, 1272–1277.
58. Saha,A., Wittmeyer,J. and Cairns,B.R. (2005) Chromatin remodeling through directional DNA translocation from an internal nucleosomal site. *Nat. Struct. Mol. Biol.*, **12**, 747–755.
59. Czaja,W., Mao,P. and Smerdon,M.J. (2014) Chromatin remodelling complex RSC promotes base excision repair in chromatin of Saccharomyces cerevisiae. *DNA Repair (Amst.)*, **16**, 35–43.
60. Menoni,H., Shukla,M.S., Gerson,V., Dimitrov,S. and Agelov,D. (2012) Base excision repair of 8-oxoG in dinucleosomes. *Nucleic Acids Res.*, **40**, 692–700.
61. Nakanishi,S., Prasad,R., Wilson,S.H. and Smerdon,M. (2007) Different structural states in oligonucleosomes are required for early versus late steps of base excision repair. *Nucleic Acids Res.*, **35**, 4313–4321.
62. Kaplan,N., Moore,I., Fondufe-Mittendorf,Y., Gossett,A.J., Tillo,D., Field,Y., Hughes,T.R., Lieb,J.D., Widom,J. and Segal,E. (2010) Nucleosome sequence preferences influence in vivo nucleosome organization. *Nat. Struct. Mol. Biol.*, **17**, 918–920.
63. Widom,J. (2001) Role of DNA sequence in nucleosome stability and dynamics. *Q. Rev. Biophys.*, **34**, 269–324.
64. Mao,P., Wyrick,J.J., Roberts,S.A. and Smerdon,M.J. (2017) UV-induced DNA damage and mutagenesis in chromatin. *Photochem. Photobiol.*, **93**, 216–228.
65. Segal,E. and Widom,J. (2009) What controls nucleosome positions? *Trends Genet.*, **25**, 335–343.